Flow Characterization Studies of the 10-MW TP3 Arc-Jet Facility: Probe Sweeps

Tahir Gökçen* and Antonella I. Alunni†
AMA Inc., NASA Ames Research Center, Moffett Field, CA 94035

This paper reports computational simulations and analysis in support of calibration and flow characterization tests in a high enthalpy arc-jet facility at NASA Ames Research Center. These tests were conducted in the NASA Ames 10-MW TP3 facility using flat-faced stagnation calorimeters at six conditions corresponding to the steps of a simulated flight heating profile. Data were obtained using a conical nozzle test configuration in which the models were placed in a free jet downstream of the nozzle. Experimental surveys of arc-jet test flow with pitot pressure and heat flux probes were also performed at these arc-heater conditions, providing assessment of the flow uniformity and valuable data for the flow characterization. Two different sets of pitot pressure and heat probes were used: 9.1-mm sphere-cone probes (nose radius of 4.57 mm or 0.18 in) with null-point heat flux gages, and 15.9-mm (0.625 in) diameter hemisphere probes with Gardon gages. The probe survey data clearly show that the test flow in the TP3 facility is not uniform at most conditions (not even axisymmetric at some conditions), and the extent of non-uniformity is highly dependent on various arc-jet parameters such as arc current, mass flow rate, and the amount of cold-gas injection at the arc-heater plenum. The present analysis comprises computational fluid dynamics simulations of the nonequilibrium flowfield in the facility nozzle and test box, including the models tested. Comparisons of computations with the experimental measurements show reasonably good agreement except at the extreme low pressure conditions of the facility envelope.

Nomenclature

c_i	=	species mass fraction for species *i*
D_e	=	nozzle exit diameter, cm (or in)
h	=	enthalpy, MJ/kg
h_o	=	total enthalpy, MJ/kg
h_{ob}	=	mass-averaged total enthalpy (or bulk enthalpy), MJ/kg
h_{ocl}	=	centerline total enthalpy, MJ/kg
I	=	arc current, A
M	=	Mach number
$\dot{m}$	=	mass flow rate, kg/s
p	=	pressure, kPa
p_{box}	=	test box pressure, torr
p_{midc}	=	arc-heater mid-column pressure, kPa
p_o	=	total pressure, kPa
p_s	=	surface pressure, kPa
p_{t2}	=	pitot pressure, kPa
q_s	=	surface heat flux, W/cm^2
q_{HWFC}	=	hot-wall full-catalytic heat flux, W/cm^2
r_c	=	model corner radius, m
r_n	=	nose radius, m
s	=	arc-length coordinate or the survey probe location, m
T	=	temperature or translational-rotational temperature, K

* Senior Research Scientist, MS 230-2, Associate Fellow AIAA
† Research Scientist, MS 234-1, Member AIAA

T_v = vibrational-electronic temperature, K
u = axial velocity component, m/s
V = arc voltage, V
x_{ml} = model location from the nozzle exit plane, cm
δ = boundary layer thickness based on total enthalpy profile, cm
ρ = density, kg/m^3

I. Introduction

Arc-jet facilities provide the primary means to study the performance of various types of thermal protection systems (TPS) used on the outer surfaces of spacecraft in an aerothermodynamic heating environment. In a high enthalpy arc-jet facility, a test gas, usually air or a mixture of nitrogen, oxygen and argon, is passed through an electric arc discharge where the energy is added to the flow. The test gas is then expanded through a converging-diverging nozzle into an evacuated test chamber to produce high-enthalpy supersonic or hypersonic flow. NASA Ames Research Center (ARC) has four arc-jet facilities within its Arc-Jet Complex.[1] One of these arc-jet facilities, the Aerodynamic Heating Facility (AHF), was recently upgraded to run with the 10-MW constricted arc heater, named the TP3, which was formerly known as the TP2 when operated at Johnson Space Center.[2] The TP3 currently operates with a test gas mixture of pure nitrogen and variable oxygen without argon gas, and in the future it is expected to run with mixtures of nitrogen and carbon dioxide.[3]

One important testing capability of the 10-MW TP3 facility is its ability to simulate various heating profiles in time representative of hypersonic flight. For the present tests, a heating profile was broken into seven independent steps where each step was calibrated using flat-faced calorimeters for its centerline conditions prior to a flight profile run, and subsequently the heating profile simulation was carried out in a single arc-jet run. Since the facility configuration is fixed, achieving the wide range of conditions needed in the heating profile simulation requires that the facility operate at the extremes of its operating envelope. Computational fluid dynamics (CFD) simulations for these tests are performed to provide accurate estimates of the test environment parameters. The centerline total enthalpy of the test flow is estimated using CFD simulations that reproduce measured facility and calorimeter data. For each step of the heating profile, surveys of arc-jet test flow with pitot and heat flux probes were performed for flow characterization. Two different sets of pitot and heat flux probes were used: 9.1-mm diameter sphere-cone probes with null-point heat flux gages and 15.9-mm diameter hemisphere probes with Gardon gages. The paper describes the computational approach to determine centerline total enthalpy, then presents comparisons of computations with the probe survey data.

II. Arc-Jet Facility and Tests

The AHF at ARC, with its 10-MW TP3 constricted arc heater configuration, is designed to operate with a set of conical nozzles. All of the nozzles have the same inlet diameter of 10.16 cm (4 in), and the same throat diameter of 5.715 cm (2.25 in). Nozzle exit diameters range from 12.7 cm to 101.6 cm (5, 7.5, 10, 20, and 40 in). The diverging section of each nozzle has a half-angle of 15°.

The present test data were obtained in three arc-jet test series conducted over a period of two years in the TP3 7.5-inch diameter conical nozzle. In the first test series, AHF 307 tests conducted in 2014, a flight heating profile was simulated in the arc-jet stream using 10.16-cm diameter flat-faced models. The heating profile was achieved through 7 steps (6 arc-heater conditions, with step 1 condition repeated as step 6 condition). Before performing flight profile runs, each step was calibrated separately for its centerline conditions with 10.16-cm diameter flat-faced slug calorimeters (the same shape as the test article) located 15.24 cm away from the nozzle exit. The shoulder region of the flat-faced models is rounded to the cylindrical sides (r_c/D = 3/32). In addition, the pitot and null-point heat flux surveys of the nozzle jet in the test section were done at the same nominal arc-heater conditions and at the same distance from the nozzle exit. These surveys were performed with the 15° sphere-cone stagnation probes (r_n = 4.57 mm or 0.18 in). The sweeps to survey across the nozzle were done by moving the probes horizontally across the free jet in two directions: first from west to east, then retracting back east to west. This provides two experimental data sets for each survey sweep. The second and third test series, AHF 318 tests in 2015 and AHF 320 tests in 2016, were conducted to get additional flow characterization data using the 15.9-mm diameter hemisphere

pitot and Gardon-gage probes at the same nominal conditions as the AHF 307 tests. The 15.9-mm probes were also moved horizontally to survey the flowfield, first from east to west and then west to east across the free jet (in opposite directions of the 9.1-mm probe sweeps). Figure 1 shows photographs of the two heat flux probes used to survey the flowfield. Each of these heat flux probes is used along with pitot pressure probes of the identical shape, although not shown in Fig. 1.

Further information on the survey probes and heat flux measurement techniques can be found in Refs. 4-7, and additional information on the TP3 facility, AHF and other ARC arc-jet facilities can be found in Refs. 1-3.

(a) 9.1-mm sphere-cone probe, null-point gage

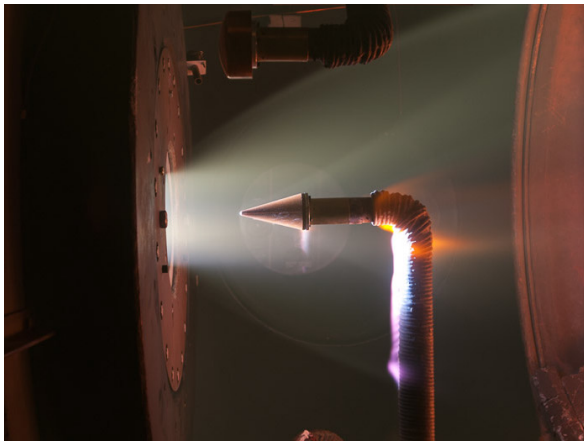

(b) AHF 307 test

(c) 15.9-mm hemisphere probe, Gardon gage

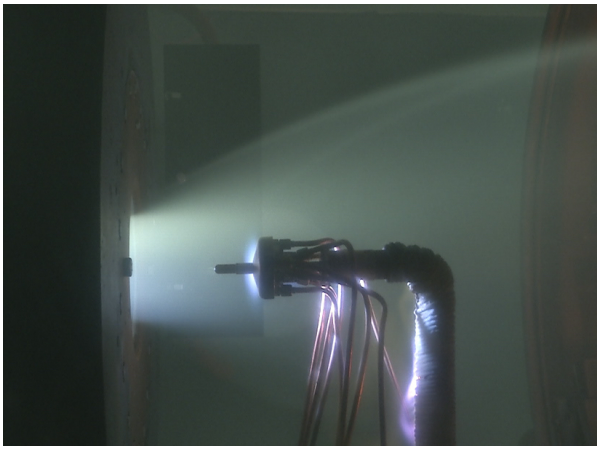

(d) AHF 320 test

Figure 1. Photographs of the survey probes used to sweep the flowfield exiting the TP3 7.5-inch nozzle.

The 10.16-cm diameter slug calorimeter data obtained in three test series are summarized in Table 1. In the TP3 arc-jet operation, similar to other arc-jet facilities, the controlled input parameters are arc current and mass flow rate, which were held constant for each condition in the three test series. Nonetheless, there were some differences in the facility performance characteristics (voltage, arc-heater mid-column pressure, estimated bulk enthalpy or arc-heater efficiency) from one test series to another, and therefore the measured slug calorimeter data varied. The facility parameters and calorimeter values listed in Table 1 are arithmetic averages of multiple (at least two) arc-jet runs. The numbers in parentheses for q_s and p_s represent the range of the data obtained. For instance, for condition 1 in AHF 307 tests, the data obtained in 17 runs were used in the averages.

Table 1. Summary of the 10.16-cm diameter flat-faced calorimeter data obtained in the TP3 7.5-inch nozzle at x_{ml} = 15.24 cm for three test series.

Test Series and Run Number	I (A)	V (V)	$\dot{m}$ (g/s)	p_{midc} (kPa)	q_s (W/cm^2)	p_s (kPa)	*Cond No.*
AHF 307 Runs 14-1–35-1	262	1264	25	25.4	58.6 (53-68)	1.74 (1.7-1.8)	1
AHF 318 Runs 11-1, 12-1	277	1169	24	24	58.0 (55-61)	1.70 (1.7-1.7)	1
AHF 320 Runs 2-1, 4-1, 5-1, 6-1	279	1179	25	27.5	60.8 (58-64)	1.62 (1.5-1.7)	1
AHF 307 Runs 11-2, 12-2	1113	3401	190	220	388 (387-388)	14.8 (14.7-14.8)	2
AHF 318 Runs 11-2, 12-2	1108	3500	190	205	495 (439-550)	14.6 (14.3-14.8)	2
AHF 320 Runs 3-2, 4-2	1110	3224	190	205	412 (399-424)	14.2 (14.0-14.4)	2
AHF 307 Runs 8-1, 9-1	1762	5187	501	558	730 (728-731)	36.0 (35.3-36.6)	3
AHF 318 Runs 11-3, 12-3	1754	5695	500	541	806 (731-880)	35.3 (35.2-35.3)	3
AHF 320 Runs 5-3, 6-3	1756	4861	500	516	593 (591-595)	33.5 (33.4-33.5)	3
AHF 307 Runs 6-1, 7-1	1214	3946	310	311	335 (330-339)	21.5 (21.5-21.5)	4
AHF 318 Runs 10-4, 13-4	1208	4063	310	298	395 (358-432)	20.5 (20.4-20.6)	4
AHF 320 Runs 3-4, 4-4	1204	3637	310	293	266 (263-268)	19.3 (19.3-19.3)	4
AHF 307 Runs 3-2, 4-1	419	1683	40	43	118 (118-118)	3.3 (3.2-3.3)	5
AHF 318 Runs 10-5, 13-5	413	1564	41	40	105 (92-118)	2.9 (2.8-2.9)	5
AHF 320 Runs 1-5, 2-5	416	1582	41	43	110 (109-110)	2.8 (2.8-2.8)	5
AHF 307 Runs 3-3, 4-2	716	3681	310	251	114 (112-115)	17.0 (16.9-17.1)	6
AHF 318 Runs 10-6, 13-6	711	4107	311	248	154 (138-170)	16.9 (16.8-17.0)	6
AHF 320 Runs 1-5, 2-5	713	3530	311	240	98 (96-100)	15.9 (15.8-15.9)	6

For conditions 1, 2, 3, and 5, no cold-gas injection at the arc-heater plenum.
For conditions 4 and 6, cold-gas injection at the plenum are 20% and 28% of the total mass flow rate, respectively.

III. Computational Approach

Computational analyses of the TP3 arc-jet tests are performed through simulation of nonequilibrium expanding flow in the arc-jet nozzle and supersonic jet, and simulation of the flow in the test box and around the test articles. For all CFD calculations, the Data Parallel Line Relaxation (DPLR) code,[8,9] a NASA Ames in-house flow solver, is used. DPLR has been employed extensively at Ames for hypersonic flight, planetary entry and arc-jet simulations. DPLR provides various options for thermophysical models and formulation. For CFD calculations presented in this paper, two-dimensional axisymmetric Navier-Stokes equations, supplemented with the equations accounting for nonequilibrium kinetic processes, are used in the formulation. The thermochemical model employed for the arc-jet flow includes five species (N_2 O_2, NO, N, O), or six species (N_2 O_2, NO, N, O, Ar) if Argon is present, and the thermal state of the gas is described by two temperatures (translational-rotational and vibrational-electronic) within the framework of Park's two-temperature model.[10]

The flowfield in an arc-jet facility, from the arc heater to the test section is very complex and three-dimensional, with various nonequilibrium processes occurring. In order to simulate the flowfield, several simplifying assumptions are made, and corresponding numerical boundary conditions are prescribed for CFD simulations. The present computational approach follows our earlier work,[11-12] and it is also briefly described here.

Simulations of the TP3 arc-jet facility flow are started from the nozzle inlet. The total enthalpy and its radial profile at the inlet are prescribed based on the facility and calibration data, and the flow properties at the inlet are assumed to be in thermochemical equilibrium. Measured facility data, namely, the total pressure, mass flow rate, and test box pressure, are used as boundary conditions. The calibration data obtained include stagnation calorimeter heat flux and pressure in the freestream. All metallic surfaces, water-cooled nozzle walls, and calorimeter model surfaces (copper slug or Gardon gages), are assumed to be fully catalytic to recombination reactions of atomic oxygen and nitrogen at a constant temperature of 500 K. The test box is included in CFD simulations, primarily to account for the free jet expansion formed by the under-expanded flow exiting the nozzle to the test box and its potential effects on model flowfields. The jet expansion within the test box is primarily determined by the test box static pressure, which is one of the facility measurements and is prescribed as a boundary condition. Further details of the computational approach can be found in Ref. 12.

IV. Computational Simulations

Stagnation calorimeters are used to calibrate the test conditions, and to infer the centerline total enthalpy of the arc-jet flow. First, one flat-faced stagnation model simulation is presented in detail, and CFD-estimated flowfield parameters are summarized. Then, comparisons of computations with the pitot pressure and heat flux surveys obtained in the TP3 7.5-inch nozzle are presented.

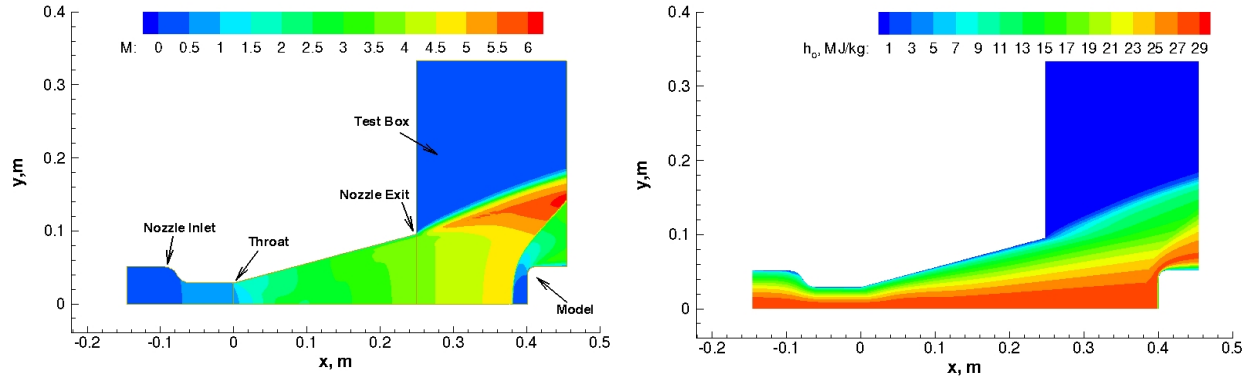

(a) Mach number **(b) total enthalpy**

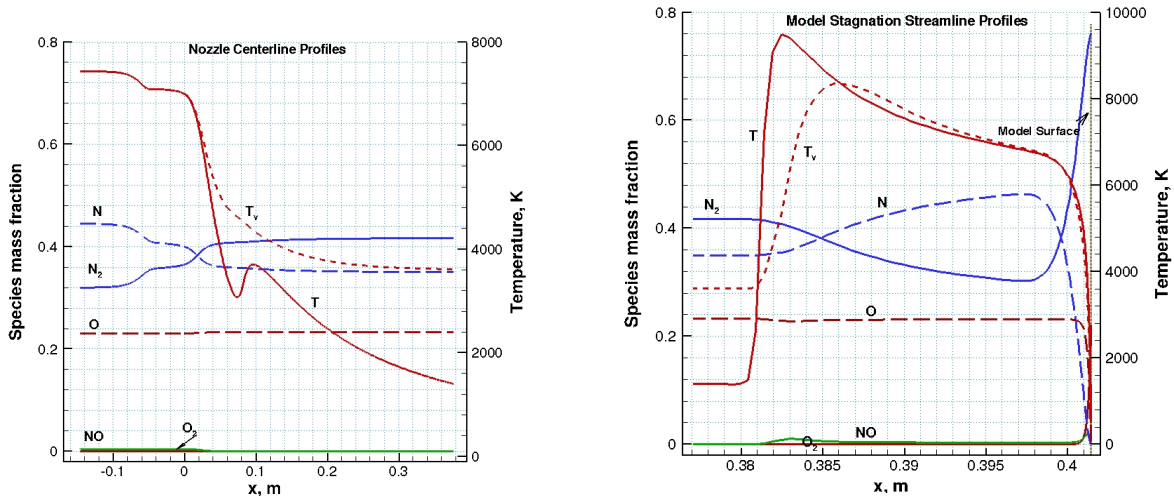

(c) nozzle centerline **(d) stagnation streamline**

Figure 2. Computed TP3 7.5-inch nozzle flowfield including the test box and a 10.16-cm diameter flat-faced calorimeter model: $\dot{m}$ = 190 g/s, parabolic enthalpy profile, h_{ob} = 17.6 MJ/kg, h_{ocl} = 28.8 MJ/kg, p_{box} = 2 torr.

A. Stagnation calorimeter model simulations

The primary objective of the stagnation model calculations is to estimate the centerline total enthalpy of the arc-jet flow consistent with the facility and calorimeter measurements. As an illustration of a typical axisymmetric simulation, Fig. 2 shows a computed TP3 7.5-inch nozzle flowfield including the test box and a stagnation calorimeter model. Because of the nonequilibrium expansion process in arc-jet nozzles, the chemical composition freezes near the throat where the flow is dissociated and vibrationally excited. As shown in Fig. 2c, the computations predict that, as expected, the flow is chemically and vibrationally frozen before it reaches the nozzle exit. Note that oxygen remains fully dissociated within the entire flowfield except in the boundary layer near the walls, while nitrogen is partially dissociated. It should be pointed out that the translational temperature rise just downstream of the throat in Fig. 2c is due to a weak oblique shock formation resulting from this particular nozzle throat design, and it is present in all simulations.

At the nozzle inlet, uniform pressure and a non-uniform parabolic enthalpy profile are specified such that the centerline calibration data are reproduced with the computations. Figure 3 shows the inlet profiles of total enthalpy and mass flux and resulting equilibrium species mass fractions and other flow properties prescribed for this case.

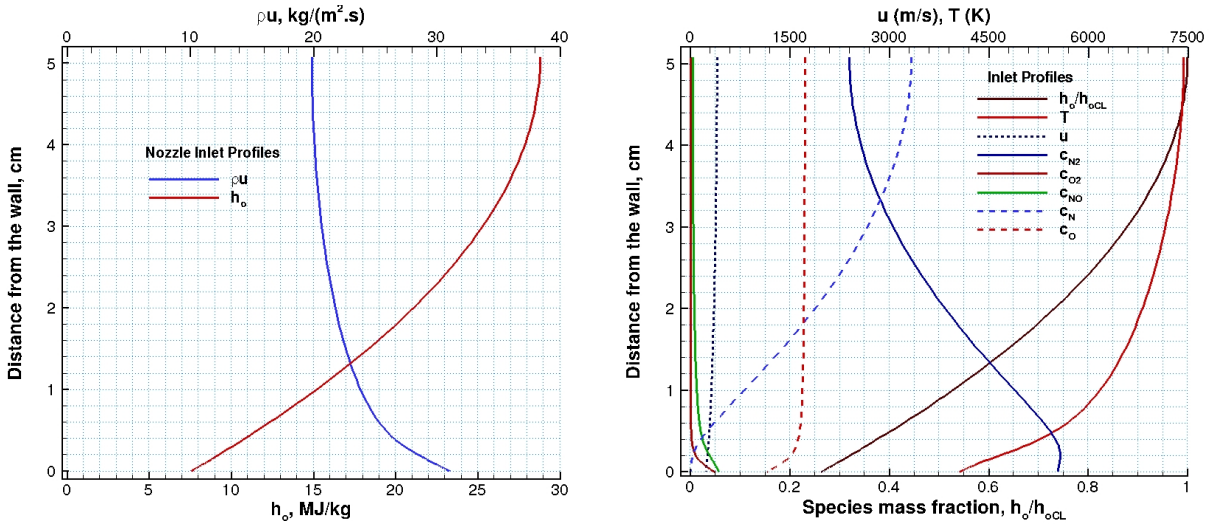

(a) **(b)**

Figure 3. Inlet profiles prescribed to reproduce the 10.16-cm diameter flat-faced calorimeter data. TP3 7.5–inch nozzle flow: $\dot{m}$ = 190 g/s, parabolic enthalpy profile, h_{ob} = 17.6 MJ/kg, h_{ocl} = 28.8 MJ/kg.

Figure 4 shows corresponding computed model surface quantities for this case. It is important to reproduce both experimental surface pressure and heat flux in order to estimate the centerline total enthalpy from CFD simulations. Note that the estimation of centerline total enthalpy from CFD simulations this way is analogous to the ASTM standard E637-05,[13] except that the calorimeter surface heat flux and pressure are predicted by CFD simulations, replacing the heat transfer theory used in the standard.

A summary of the facility parameters and CFD-estimated enthalpies for the six conditions based on the calibration data obtained in AHF 307 test series is given in Table 2. Since the slug calorimeter data obtained for condition 3 and 4 in AHF 320 tests were more than 15% different from those of AHF 307 tests, additional CFD calculations were performed to estimate the centerline total enthalpy values for AHF 320 tests, which are also given in Table 2. Although the flight profile simulation and its results are outside the scope of this paper, the hot-wall heat flux values, computed using radiative equilibrium boundary conditions, are provided to make comparisons of the simulated arc-jet heating profile with the corresponding flight heating profile.

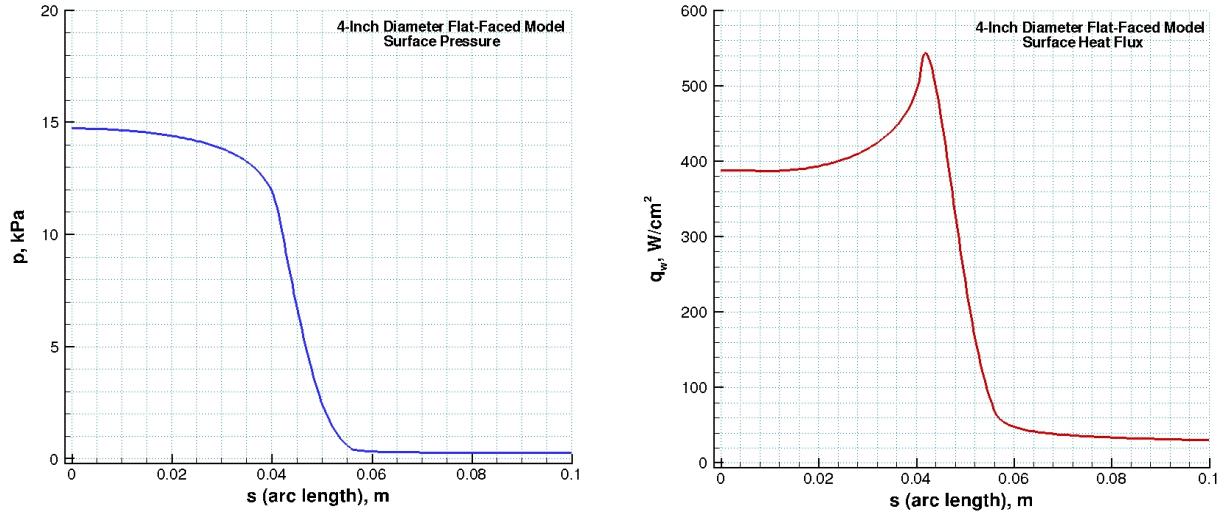

(a) pressure **(b) heat flux**

Figure 4. Computed surface pressure and heat flux distributions for the flat-faced model. TP3 7.5-inch nozzle flow: $\dot{m}$ = 190 g/s, h_{ob} = 17.6 MJ/kg, h_{ocl} = 28.8 MJ/kg. Test data (AHF 307 Runs 11-2, 12-2): 388 W/cm^2 and 14.8 kPa.

Table 2. Summary of nominal facility parameters, calibrated conditions, and CFD estimates for a flight heating profile simulation: 10.16-cm diameter flat-faced calorimeter data obtained in the TP3 7.5-inch nozzle at x_{ml} = 15.24 cm.

Test Series: AHF 307	***I*** **(A)**	***V*** **(V)**	$\dot{m}$ **(g/s)**	p_{midc} **(kPa)**	q_s **(W/cm^2)**	p_s **(kPa)**	h_{ob} **(MJ/kg) CFD**	h_{ocl} **(MJ/kg) CFD**	q_{HWFC} **(W/cm^2) CFD**	***Cond No.***
Runs 14-1–35-1	262	1264	25	25.4	58.6	1.74	11.8	13.8	51.5	1
Runs 11-2, 12-2	1113	3401	190	220	388	14.8	17.6	28.8	349	2
Runs 8-1, 9-1	1762	5187	501	558	730	36.0	16.4	34.1	497	3
Runs 6-1, 7-1	1214	3946	310	311	335	21.5	13.6	21.9	292	4
Runs 3-2, 4-1	419	1683	40	43	118	3.3	15.4	19.6	104	5
Runs 3-3, 4-2	716	3681	310	251	114	17.0	7.5	9.4	89	6
AHF 320										
Runs 5-3, 6-3	1756	4861	500	516	593	33.5	13.9	29.9	N/A	3
Runs 3-4, 4-4	1204	3637	310	293	266	19.3	10.3	18.8	N/A	4

Conditions 4 and 6 include cold-gas injection at the plenum, 20% and 28% of the total mass flow rate, respectively.

B. Comparisons with survey data

Direct comparisons of CFD simulations with the survey data present a number of challenges. While the data obtained from the pitot pressure surveys are used as quantitative data, the heat flux measurements from the null-point and Gardon-gage surveys are used as qualitative data since they were not consistent with the slug calorimeter data. Therefore, only normalized distributions of the heat flux measured by the survey probes can be used in comparisons with computations. Furthermore, direct comparions would require three-dimensional CFD simulations of flowfields around the survey probes at several locations in the test section.

For the present paper, approximate comparisons are made based on the computed CFD flowfields. Quantitative pitot pressure comparisons are based on the computed flowfield and shock relations (pressure, Mach number, frozen

flow). For normalized heating distribution comparisons, the heat flux from the null-point and Gardon-gage probes is assumed to be proportional to $h_o\, p_{t2}^{1/2}$, and corresponding computations are based on the CFD flowfield.

Comparisons of computations with the pitot and null-point heat flux survey data will be presented for the six conditions used in the heating profile simulation. Note that for each condition, the centerline total enthalpy value is set such that centerline stagnation calorimeter data, surface pressure and heat flux, are reproduced. The survey data were obtained in separate arc-jet runs but at the same nominal facility conditions listed in Table 1. Also, note that the pitot survey data were taken during a different run from the null-point or Gardon-gage heat flux surveys, but at nominally the same arc heater settings. The probe survey data and comparisons with computations are presented in Figs. 5-21.

i. Condition 1

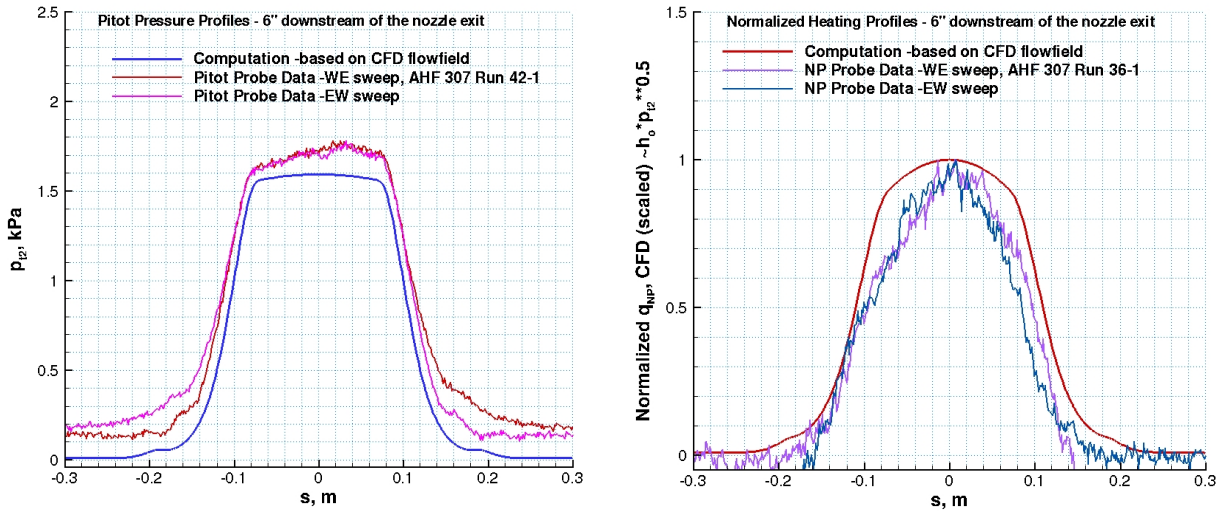

(a) pitot pressure **(b) normalized heat flux**

Figure 5. Comparisons of computations with the pitot pressure and null-point heat flux survey data for condition 1 (step 1 and step 6). TP3 7.5-inch nozzle flow: $\dot{m}$ = 25 g/s, h_{ob} = 11.8 MJ/kg, h_{ocl} = 13.8 MJ/kg, p_{box} = 0.05 torr.

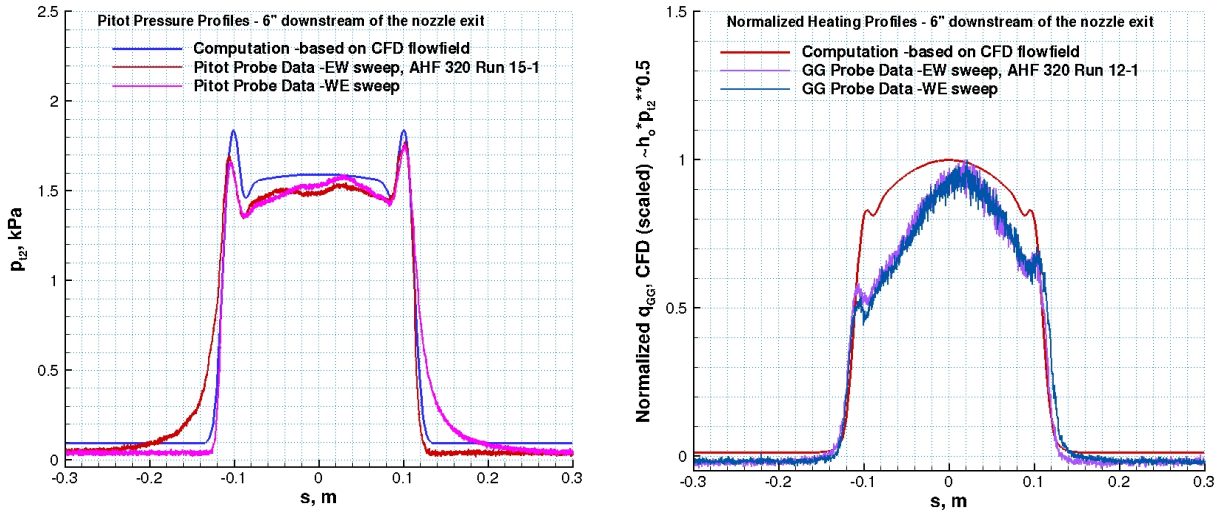

(a) pitot pressure **(b) normalized heat flux**

Figure 6. Comparisons of computations with the pitot pressure and Gardon-gage heat flux survey data for condition 1. TP3 7.5-inch nozzle flow: $\dot{m}$ = 25 g/s, h_{ob} = 11.8 MJ/kg, h_{ocl} = 13.8 MJ/kg, p_{box} = 0.7 torr.

The first condition (step 1 and step 6) represents a facility condition at an extremely low mass flow rate and moderate enthalpy. There is no plenum cold gas injection. Figure 5 shows comparisons of computations with the pitot pressure and null-point heat flux survey data using the 9.1-mm sphere-cone probes. Note that while the obtained sweep data are mostly repeatable in both sweep directions, both pitot and heat flux survey data are not symmetric with respect to the nozzle centerline. It is not clear what the source of this asymmetry in the flow is, and obviously any observed asymmetry in the flow cannot be reproduced by an axisymmetric formulation. Also note that there was an incomplete recovery in the pitot data to the test box pressure, most likely because the pitot survey probe was moving too fast to equilibrate at these low pressures. It was found that the dwell time for the probes to traverse the jet was an important variable, especially at these low pressures. For some runs in AHF 318 tests, the probe speeds were too fast to get any reliable data. Repeatability and probe dwell time sensitivity for Gardon gage surveys for all six conditions are given in the Appendix (Figs. A1-A6).

Figure 6 shows the comparisons of computations with the pitot pressure and Gardon-gage heat flux survey data using the 15.9-mm hemisphere probes. First, it should be noted that the features in the pitot and heat flux surveys at s ~ ±0.12 correspond to the nozzle jet boundary, the location of which is primarily determined by the test box pressure. The striking difference in the width of the jet (Fig. 6a-b vs. Fig. 5a-b) is caused by the higher test box pressure during AHF 320 runs. Equilibration of the pitot pressure is an important factor, especially for the 15.9-mm probes that required longer times to reach a steady-state condition. The asymmetry observed in the heating profile is more pronounced than the results from the null-point probe for AHF 307. For both instances of the condition 1 comparison, the computed heating profile is less peaked near the centerline than the probe surveys indicate. Although it is possible to change the enthalpy profile at the nozzle inlet to improve the comparisons, an increase in the prescribed mass flow rate would be needed. Note that the mass flow rate is extremely low and at the minimum for this facility. The measured mass flow rate for this condition may not be as accurate as the other conditions at much higher mass flow rates.

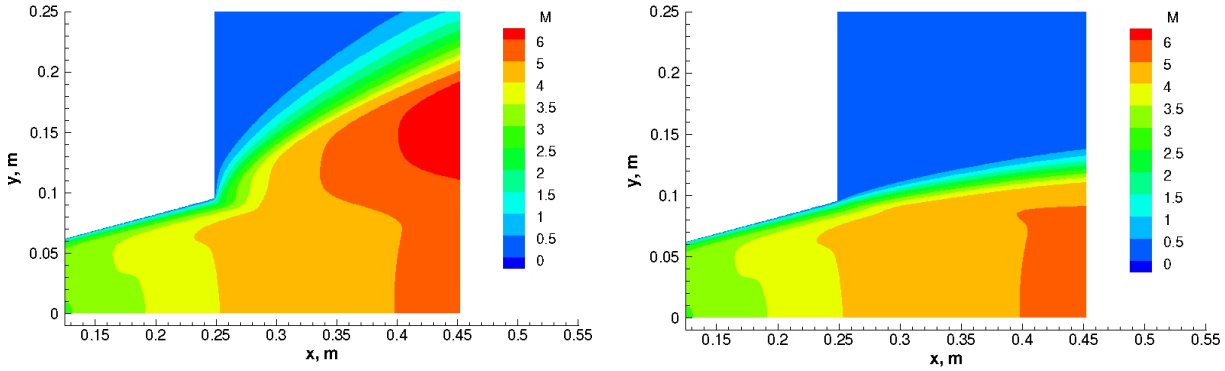

(a) p_{box} = 0.05 torr **(b) p_{box} = 0.7 torr**

Figure 7. Effects of the test box pressure on computed Mach number contours for condition 1. TP3 7.5-inch nozzle flow: $\dot{m}$ = 25 g/s, h_{ob} = 11.8 MJ/kg, h_{ocl} = 13.8 MJ/kg.

For the CFD simulations shown in Figs. 5 and 6, all boundary conditions are the same except for the different test box pressures that are prescribed, consistent with the facility data. Figure 7 shows the computed Mach number contours near the nozzle exit and supersonic jet at two prescribed test box pressures. Clearly, for the higher test box pressure, the expansion of the jet exiting the nozzle is contained, as the width of the jet is primarily controlled by the box pressure. The axial location for both survey probes is approximately x = 0.402 m.

ii. Condition 2

The second condition (step 2) represents a facility condition at an intermediate mass flow rate, with relatively high enthalpy and without plenum gas injection. Figures 8 and 9 show comparisons of computations with the pitot pressure and heat flux survey data for condition 2. In Fig. 8, CFD simulations reproduce the the pitot pressure and null-point data quite well. On the other hand, although the pitot pressure data are reproduced reasonably well in

Fig. 9a, the Gardon-gage heat flux data show a more peaked distribution than the computations. Note that the extent of asymmetry in both pitot and heat flux data (more noticeable in Fig. 9b) is much smaller than in the first condition, within the measurement fluctuations. Note also that there appears to be some variation in the pitot pressure near the nozzle centerline, possibly resulting from weak wave interactions in the supersonic jet.

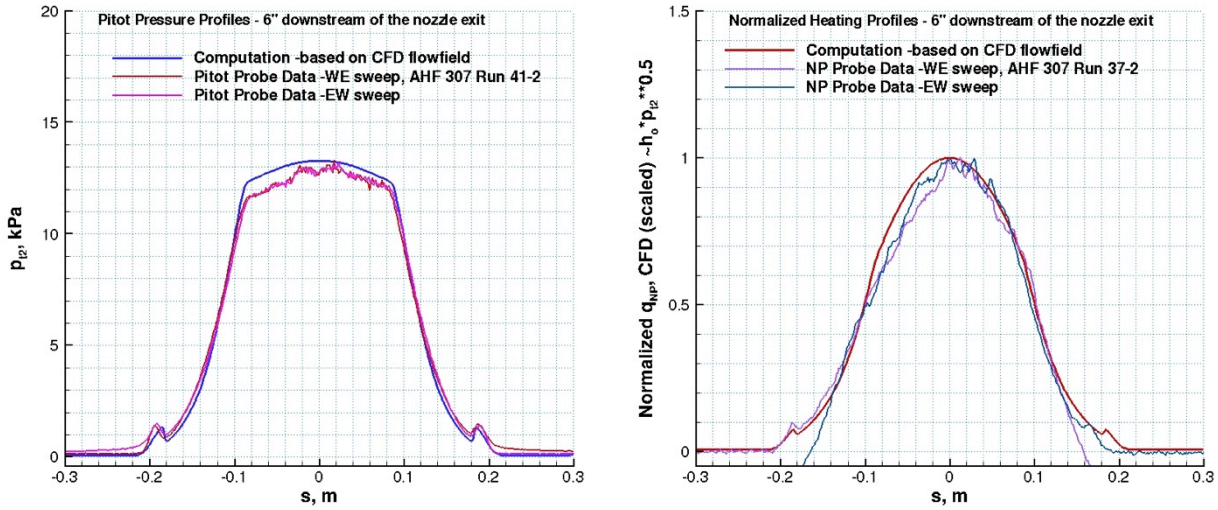

(a) pitot pressure **(b) normalized heat flux**

Figure 8. Comparisons of computations with the pitot pressure and null-point heat flux survey data for condition 2 (step 2). TP3 7.5-inch nozzle flow: $\dot{m}$ = 190 g/s, h_{ob} = 17.6 MJ/kg, h_{ocl} = 28.8 MJ/kg, p_{box} = 0.4 torr.

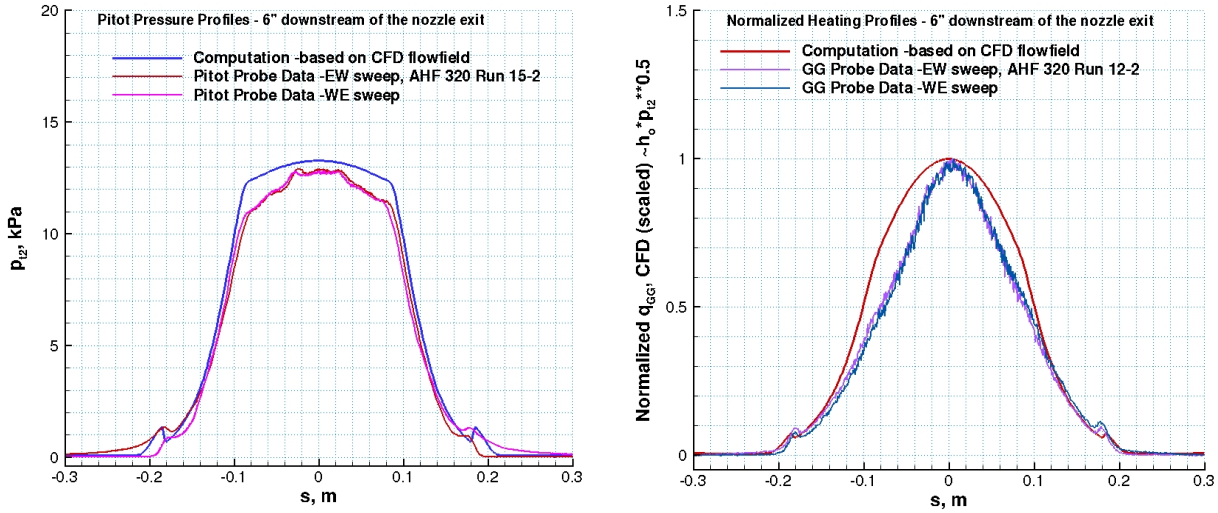

(a) pitot pressure **(b) normalized heat flux**

Figure 9. Comparisons of computations with the pitot pressure and Gardon-gage heat flux survey data for condition 2. TP3 7.5-inch nozzle flow: $\dot{m}$ = 190 g/s, h_{ob} = 17.6 MJ/kg, h_{ocl} = 28.8 MJ/kg, p_{box} = 0.4 torr.

iii. Condition 3

The third condition (step 3) represents the maximum facility condition in terms of both mass flow rate and arc current, without plenum gas injection. Figures 10 and 11 show comparisons of computations with the pitot pressure and heat flux survey data for condition 3. As mentioned earlier, since the calorimeter data for this condition in AHF

320 tests varied significantly from the previous tests, separate CFD simulations are performed to estimate the centerline total enthalpy. The computations in Fig. 11 are different from those in Fig. 10, although the normalized heating distributions look similar (the centerline-to-bulk enthalpy ratios are similar, 2.08 vs 2.15). For this case, the asymmetric distributions in both pitot and heat flux data are observed. The variation in the pitot pressure near the nozzle centerline is also more pronounced in comparison with condition 2, again possibly because of weak wave interactions in the supersonic jet.

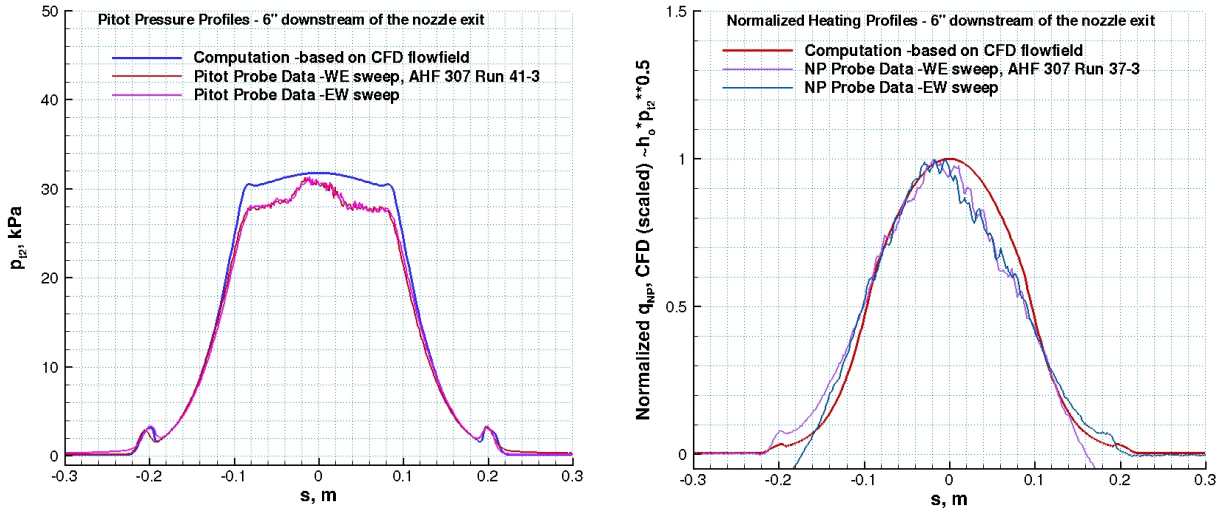

(a) pitot pressure **(b) normalized heat flux**

Figure 10. Comparisons of computations with the pitot pressure and null-point heat flux survey data for condition 3 (step 3). TP3 7.5-inch nozzle flow: $\dot{m}$ = 501 g/s, h_{ob} = 16.4 MJ/kg, h_{ocl} = 34.1 MJ/kg, p_{box} = 1 torr.

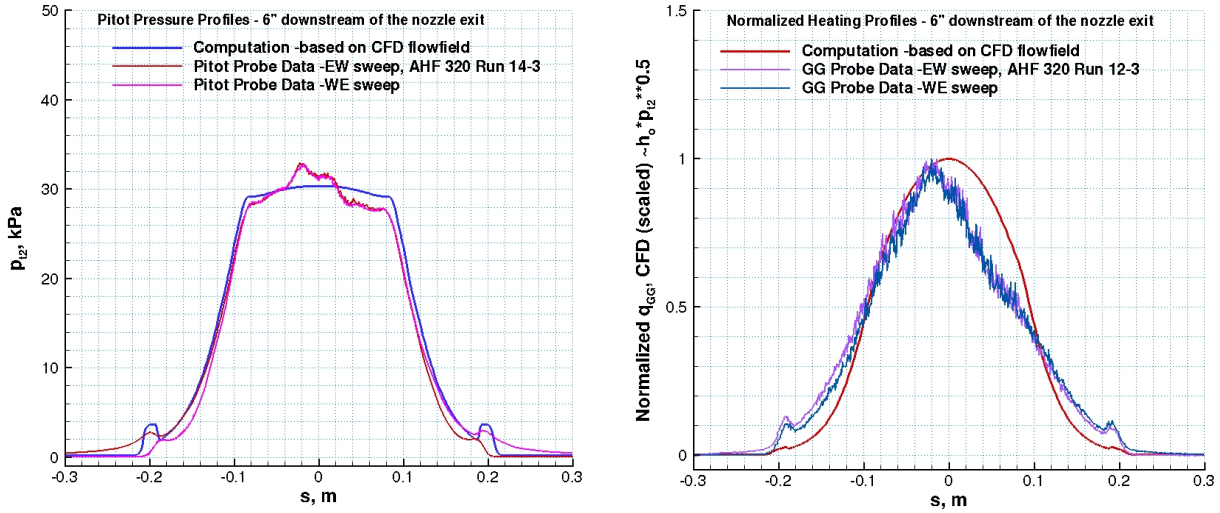

(a) pitot pressure **(b) normalized heat flux**

Figure 11. Comparisons of computations with the pitot pressure and Gardon-gage heat flux survey data for condition 3. TP3 7.5-inch nozzle flow: $\dot{m}$ = 500 g/s, h_{ob} = 13.9 MJ/kg, h_{ocl} = 29.9 MJ/kg, p_{box} = 1 torr (based on AHF 320 calibration data).

iv. Condition 4

The fourth condition (step 4) represents a facility condition at a relatively high mass flow rate and moderately high enthalpy with plenum gas injection of N_2 (20% of total mass flow rate). Figures 12-14 show comparisons of

computations with the pitot pressure and heat flux survey data for condition 4. Again, the calibration data for condition 4 in AHF 320 tests were different from AHF 307 and AHF 318 tests, in heat flux values greater than 20%. Separate CFD calculations are performed to estimate the centerline total enthalpy based on AHF 320 calorimeter data, as shown in Fig. 14. For this case, all of the pitot pressure survey data also show a higher pressure region near the nozzle centerline. Although this feature could plausibly be explained by some geometric imperfections in the nozzle walls upstream of the nozzle exit, the fact that it does not appear in all surveys for other conditions requires further investigation. It is important to note that all of the survey data for this condition, pitot pressure and heat flux, appear to be approximately symmetric, and they are reasonably well reproduced by the CFD simulations.

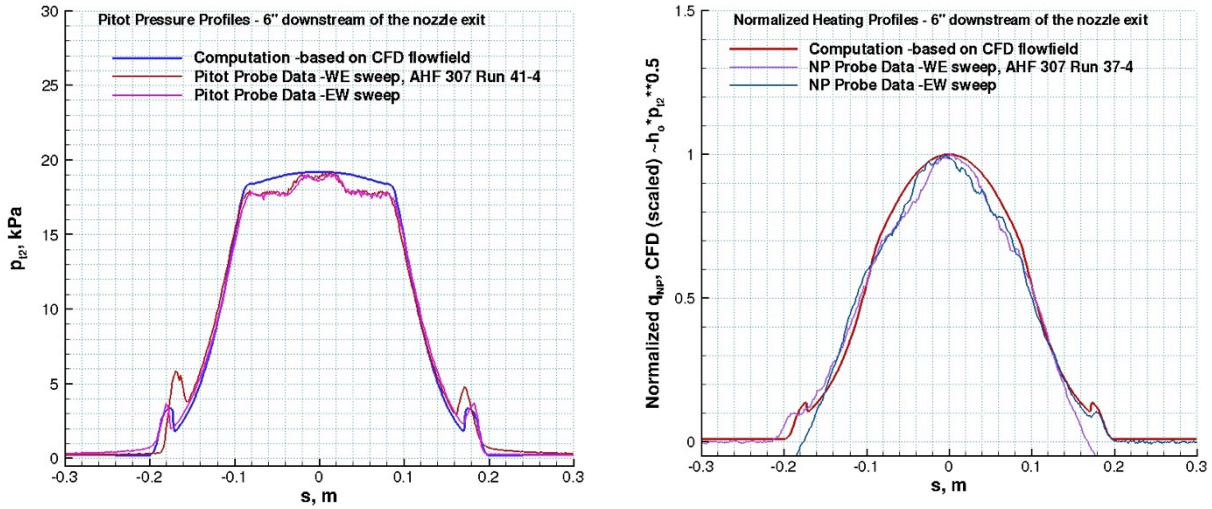

(a) pitot pressure **(b) normalized heat flux**

Figure 12. Comparisons of computations with the pitot and null-point heat flux survey data for condition 4 (step 4). TP3 7.5-inch nozzle flow: $\dot{m}$ = 310 g/s, h_{ob} = 13.6 MJ/kg, h_{ocl} = 21.9 MJ/kg, p_{box} = 1 torr.

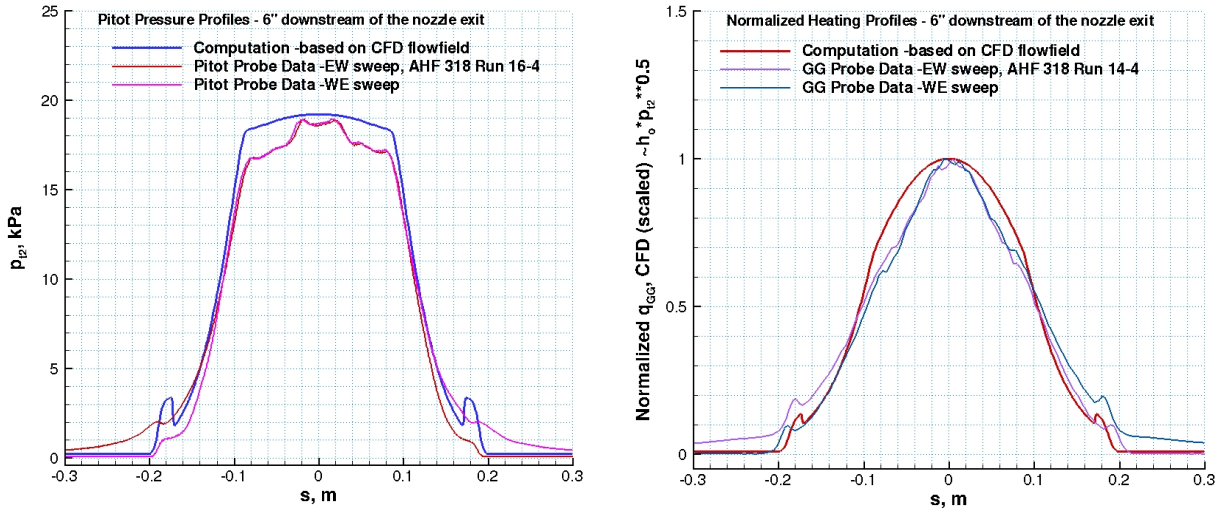

(a) pitot pressure **(b) normalized heat flux**

Figure 13. Comparisons of computations with the pitot pressure and Gardon-gage heat flux survey data for condition 4. TP3 7.5-inch nozzle flow: $\dot{m}$ = 310 g/s, h_{ob} = 13.6 MJ/kg, h_{ocl} = 21.9 MJ/kg, p_{box} = 1 torr.

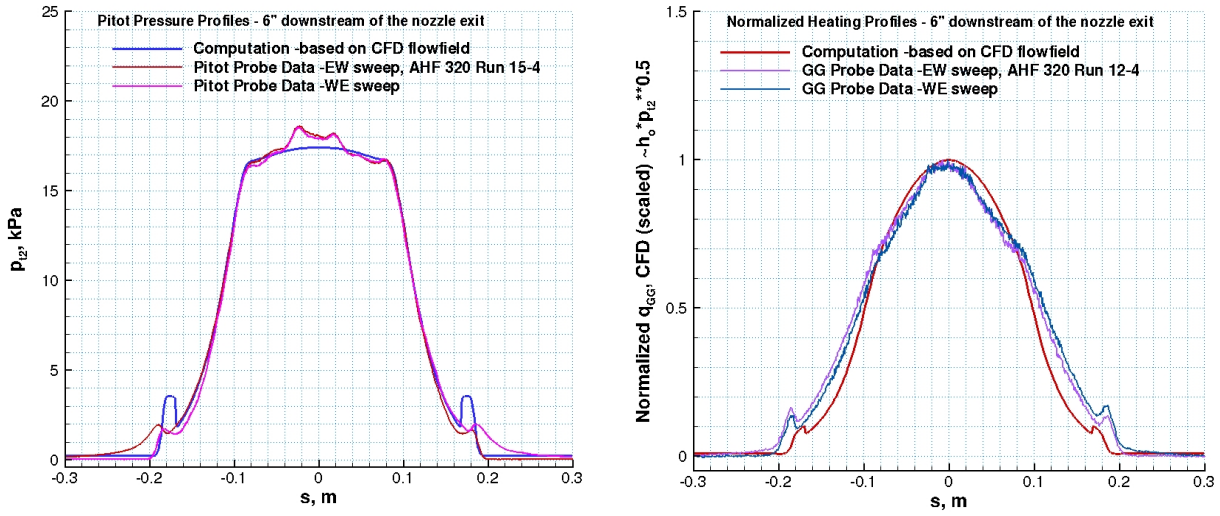

(a) pitot pressure **(b) normalized heat flux**

Figure 14. Comparisons of computations with the pitot pressure and Gardon-gage heat flux survey data for condition 4. TP3 7.5-inch nozzle flow: $\dot{m}$ = 310 g/s, h_{ob} = 10.3 MJ/kg, h_{ocl} = 18.8 MJ/kg, p_{box} = 1 torr (based on AHF 320 calibration data).

v. Condition 5

The fifth condition (step 5) represents a facility condition at a relatively low mass flow rate and moderate enthalpy. There is no plenum cold gas injection. Figures 15-17 show comparisons of computations with the pitot pressure and heat flux survey data for condition 5. There was not a complete recovery in the pitot data to the test box pressure, shown in Figs. 15 and 16. As discussed before, this is due to the probe speed being too fast to equilibrate at these lower pressures. All of the pitot and heat flux survey data are not symmetric with respect to the nozzle centerline, similar to those for the first case shown in Figs. 5-6. Also, note that the asymmetric feature (or departures from axisymmetric CFD computations in these comparions) skews to the east side (s < 0) for conditions 1 and 5 but it skews to the west side (s > 0) for condition 3. Comparisons presented in Figs. 16 and 17 highlight the effects of the test box pressure, similar to those observed in Figs. 5 and 6 for condition 1.

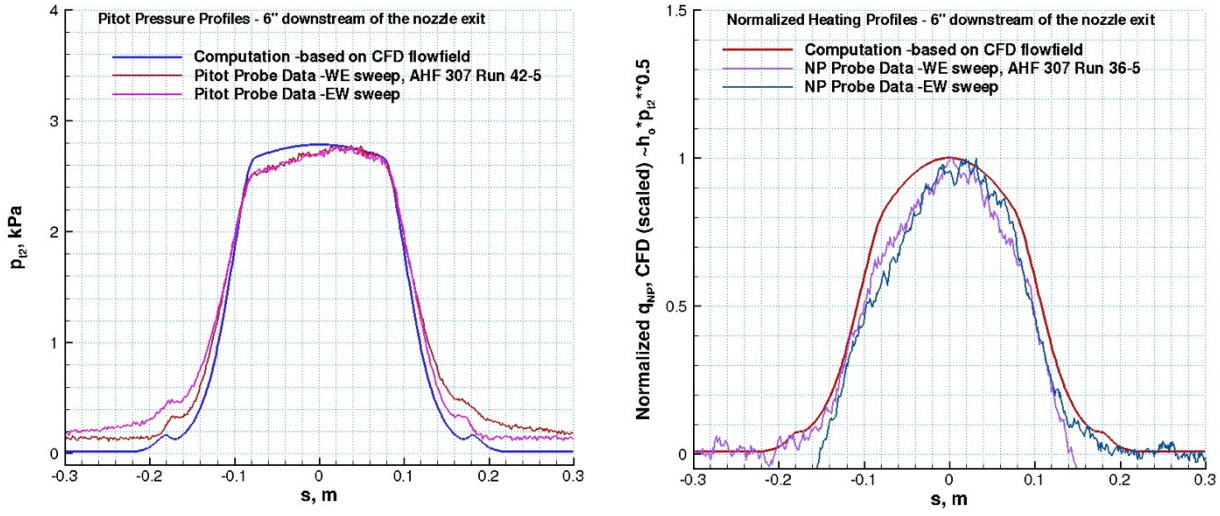

(a) pitot pressure **(b) normalized heat flux**

Figure 15. Comparisons of computations with the pitot and null-point heat flux survey data for condition 5 (step 5). TP3 7.5-inch nozzle flow: $\dot{m}$ = 40 g/s, h_{ob} = 15.4 MJ/kg, h_{ocl} = 19.6 MJ/kg, p_{box} = 0.1 torr.

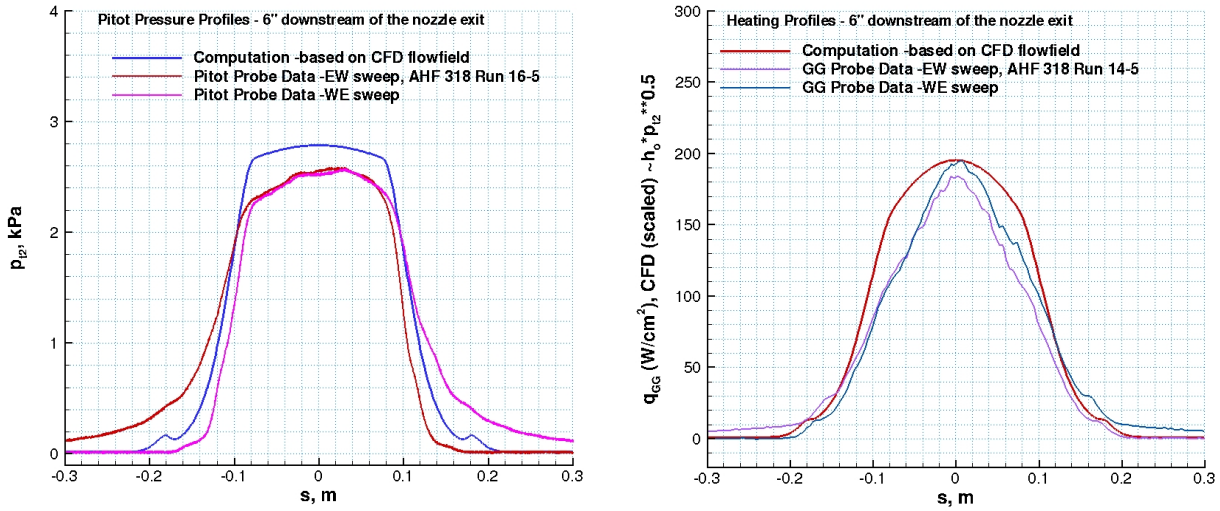

(a) pitot pressure **(b) normalized heat flux**

Figure 16. Comparisons of computations with the pitot pressure and Gardon-gage heat flux survey data for condition 5. TP3 7.5-inch nozzle flow: $\dot{m}$ = 40 g/s, h_{ob} = 15.4 MJ/kg, h_{ocl} = 19.6 MJ/kg, p_{box} = 0.1 torr.

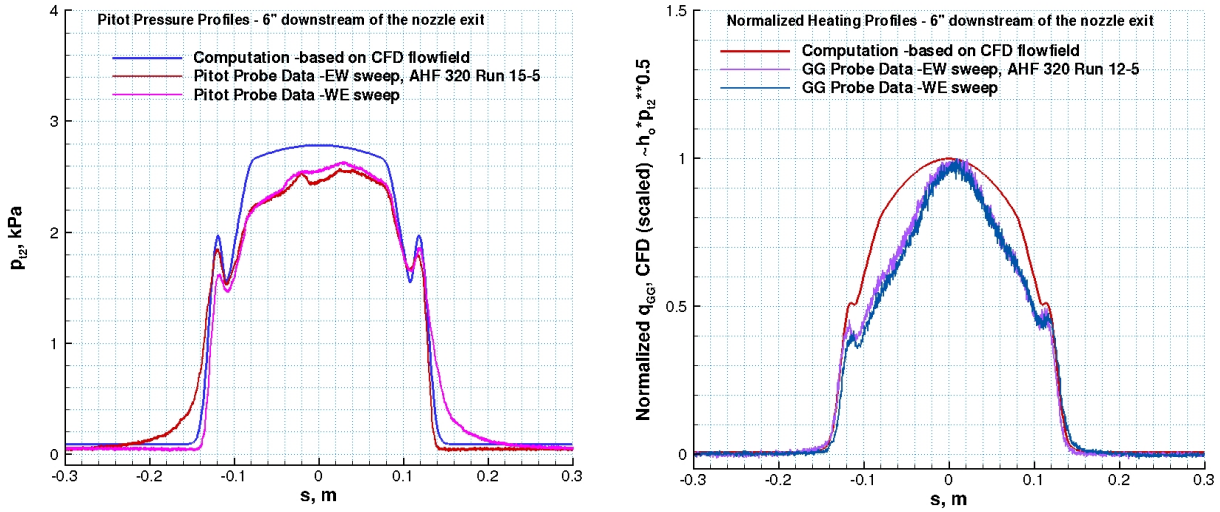

(a) pitot pressure **(b) normalized heat flux**

Figure 17. Comparisons of computations with the pitot pressure and Gardon-gage heat flux survey data for condition 5. TP3 7.5-inch nozzle flow: $\dot{m}$ = 40 g/s, h_{ob} = 15.4 MJ/kg, h_{ocl} = 19.6 MJ/kg, p_{box} = 0.7 torr.

vi. Condition 6

The sixth condition (step 7) represents a facility condition at a relatively high mass flow rate and relatively low enthalpy. The mass flow rate for this case is the same as the fourth condition but the centerline total enthalpy is much lower. The lower enthalpy is achieved through a lower arc current and more cold gas injection of N_2 at the plenum (28% of total mass flow rate). Figures 18-20 show comparisons of computations with the pitot pressure and heat flux survey data for condition 6. Again, it should be noted that the features in the pitot and heat flux surveys in Fig. 18 (at s ~ ±0.15 for pressure, and s ~ ±0.19 for heat flux) correspond to the nozzle jet boundary, the location of which is primarily determined by the test box pressure. The pressure and heat flux surveys were obtained in two separate runs at the same nominal arc-heater conditions. However, the box pressures for each run were different. One remarkable point about this case is the relatively uniform heating distributions compared with other cases presented earlier. This is in contrast to our experience with other arc-jet facilities in which observed flow non-

uniformity generally increases with increasing cold-gas injection at the plenum, possibly due to an incomplete mixing process. For this facility, the cold-gas injection at the plenum does not appear to be the primary source of non-uniform enthalpy profile. However, all of the pitot pressure survey data appear to indicate some wave interactions near the nozzle centerline, possibly caused by the cold-gas injection and mixing process. Overall, the computations are in reasonably good agreement with the survey data.

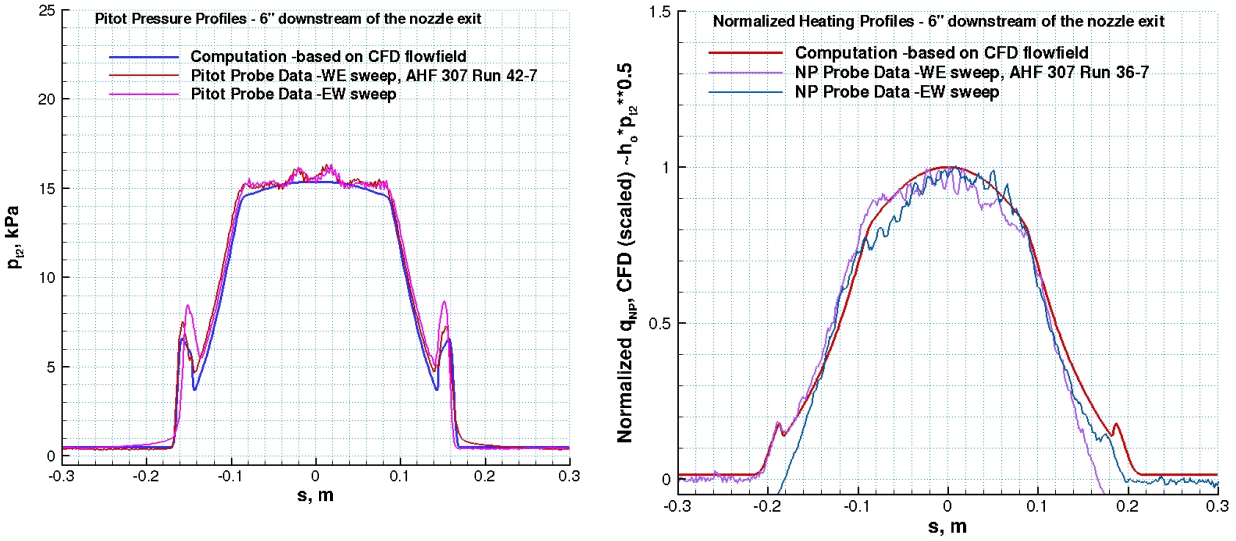

(a) pitot pressure at p_{box} = 2 torr **(b) normalized heat flux at p_{box} = 0.5 torr**

Figure 18. Comparisons of computations with the pitot and null-point heat flux survey data for condition 6 (step 7). TP3 7.5-inch nozzle flow: $\dot{m}$ = 310 g/s, h_{ob} = 7.5 MJ/kg, h_{ocl} = 9.4 MJ/kg.

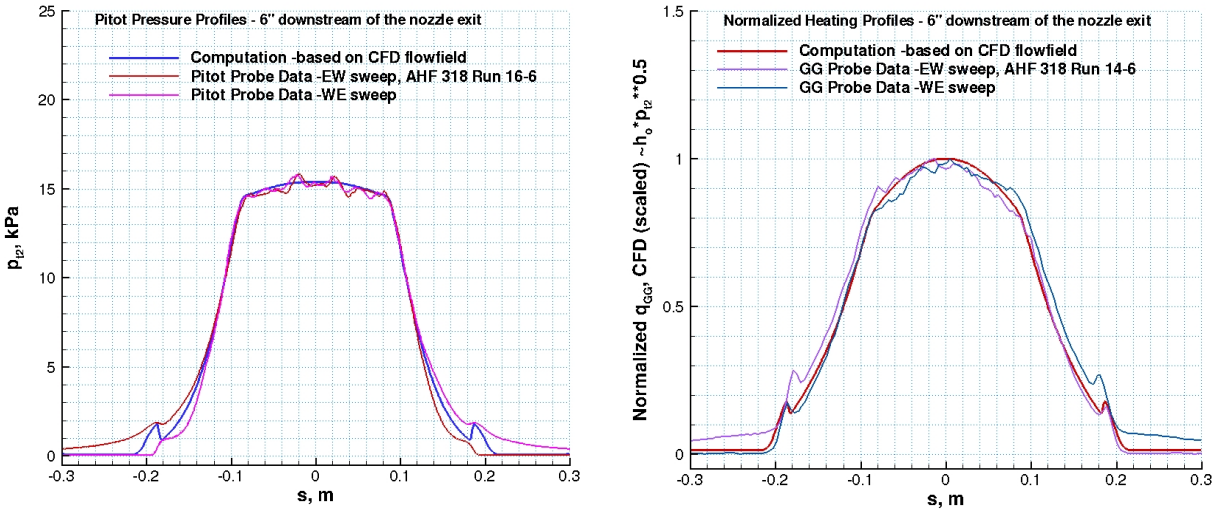

(a) pitot pressure **(b) normalized heat flux**

Figure 19. Comparisons of computations with the pitot pressure and Gardon-gage heat flux survey data for condition 6. TP3 7.5-inch nozzle flow: $\dot{m}$ = 310 g/s, h_{ob} = 7.5 MJ/kg, h_{ocl} = 9.4 MJ/kg, p_{box} = 0.5 torr.

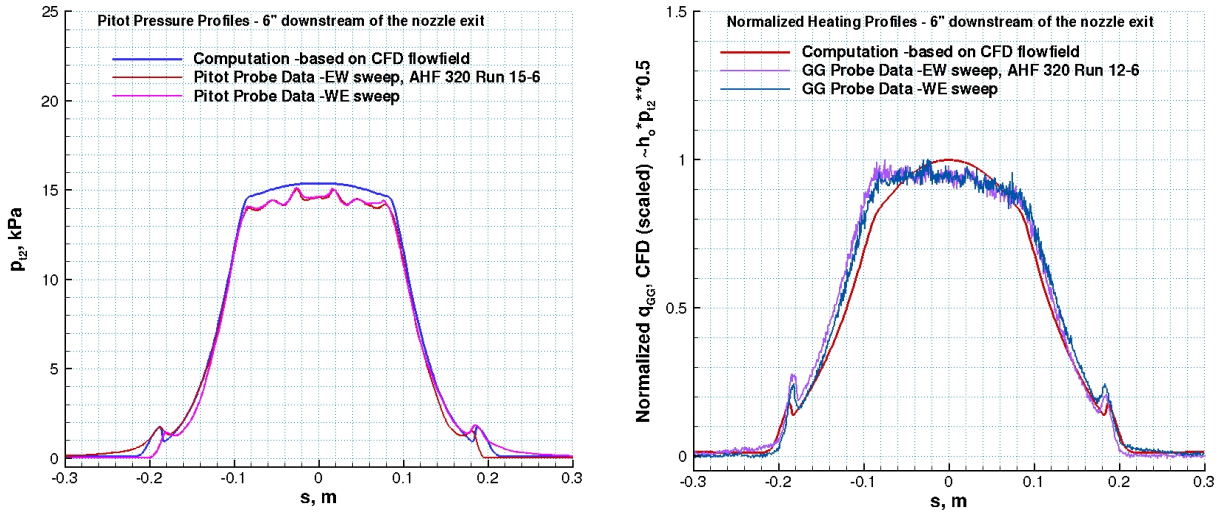

(a) pitot pressure **(b) normalized heat flux**

Figure 20. Comparisons of computations with the pitot pressure and Gardon-gage heat flux survey data for condition 6. TP3 7.5-inch nozzle flow: $\dot{m}$ = 310 g/s, h_{ob} = 7.5 MJ/kg, h_{ocl} = 9.4 MJ/kg, p_{box} = 0.5 torr.

C. Estimated Uncertainties and Calibration Issues

A complete uncertainty analysis of the heat flux and pressure measurements is not available. The slug calorimeter measurements are standard facility measurements, and based on empirical evidence (historical Ames arc-jet data with similar measurements), the heat flux measurements are estimated to be accurate to within ±15% and the pressure measurements to within ±5%. The stagnation Gardon gage calorimeters are very useful for calibration of a heating profile simulation including multiple steps since they are water-cooled. However, inconsistencies in the Gardon gage and slug calorimeter measurements were observed. For this reason, each step of the heating profile is calibrated with a slug calorimeter prior to a profile run. The heat flux measurements from the null-point gage and Gardon-gage probes are used as qualitative measurements to provide normalized distributions of heat flux. Complicating these calibration issues further, in the AHF 318 and AHF 320 test series, two slug calorimeters with different model geometries (i.e., flat-faced and iso-q shaped calorimeters) also provided data inconsistent with each other. The iso-q calorimeter heat flux data were generally higher than the flat-faced calorimeter data but the differences were not as much as expected from these two geometries. The causes of all these inconsistencies are currently being investigated. The observed non-uniformity and asymmetry in the pitot pressure and heating profiles at certain conditions may be an important contributing factor. The effects of an asymmetric freestream flow on the calorimeter flowfield, heat flux measurements and their interpretation need to be investigated. Several additional challenges remain in arc-jet flow calibration using multiple heat flux measuring devices to provide heat flux datasets consistent with each other: calibration of the null-point and Gardon gages, and reexamination of methodologies to infer the heat flux for these measurement devices.

CFD computations of arc-jet flows, as for hypersonic flight simulations, include uncertainties in many of the model input parameters. It is not possible at this time to do a complete uncertainty analysis of computed results for all of the simulation input parameters. The most important input parameter of the arc-jet test flow is the total enthalpy and its distribution at the nozzle inlet. Considering the uncertainty in the enthalpy input, prescribed inlet conditions, and other modeling parameters, the uncertainty in the heat flux predictions is estimated to be as much as ±20%. The uncertainty in surface pressure predictions is estimated to be ±5-10%.

V. Summary and Concluding Remarks

Computational simulations and analysis in support of calibration and flow characterization tests in the NASA Ames 10-MW TP3 arc-jet facility flow are reported. The test data included heat flux and pressure measurements

with stagnation calorimeters, and surveys of arc-jet test flow with pitot pressure and heat flux probes. The 10.16-cm diameter flat-faced slug calorimeter measurements are used as primary calibration data for six test conditions. Two sets of pitot pressure and heat probes were used: the 9.1-mm sphere-cone probes with null-point heat flux gages and 15.9-mm diameter hemisphere probes with Gardon gages. The probe survey data obtained at six arc-heater conditions provide assessment of the flow uniformity and valuable data for the flow characterization. Computations of the nonequilibrium flowfield in the nozzle, test box, and over the test articles, are performed. These simulations take into account nonuniformities in the total enthalpy and mass flux profiles at the nozzle inlet as well as the effects of the test box pressure on the supersonic jet, and they predict model surface pressure and heat flux measurements consistent with the set of arc-jet facility data. Computational simulations, through comparisons with the test data, provide estimates of arc-jet test environment parameters, the centerline total enthalpy being the most important test parameter.

The probe survey data clearly show that the arc-jet test flow in the TP3 facility is not uniform at most conditions, and the extent of non-uniformity is highly dependent on various arc-jet parameters such as arc current, mass flow rate (or arc heater pressure), and the amount of cold-gas injection at the arc-heater plenum. The six conditions studied are steps of a specific flight heating profile simulation and cover a wide range of facility parameters. Arc current varies from 262 A to 1762 A (from the minimum to the maximum for this facility), total mass flow rates range from 24 g/s to 501 g/s (arc-heater mid-column pressures range from 24 kPa to 558 kPa), and two conditions include cold-gas injection at the plenum. At the extremes of the facility operating envelope, i.e., at the minimum arc current and mass flow rate, and the maximum arc current and mass flow rate, the surveys indicate that the flowfield is not axisymmetric. From a TPS testing perspective, the effects of an asymmetric test flow would vary, minimal to important, depending on the test configurations and objectives (stagnation pucks, wedge plate, etc.). For flow characterization purposes, since all of the present CFD simulations assume an axisymmetric flow, effects of the observed asymmetric flows on the calorimeter measurements and their interpretation (CFD-estimated centerline total enthalpy values) remain to be investigated.

Acknowledgments

This work was funded by the NASA Orion TPS Insight/Oversight project. The arc-jet operational capability at NASA ARC is also supported by NASA-SCAP. The authors would like to thank all of the facilities staff involved in the TP3 tests, in particular, test engineers Frank C. L. Hui, J. Enrique Carballo, Erika D. Rodrigues, and Imelda Terrazas-Salinas. The support from the NASA Ames Entry Systems and Technology Division, through contract NNA15BB15C to AMA, Inc., is gratefully acknowledged.

References

[1]Terrazas-Salinas, I., and the staff of Thermophysics Facilities Branch, "Test Planning Guide for NASA Ames Research Center Arc-Jet Complex and Range Complex," A029-9701-XM3 Rev. C, Entry Systems and Technology Division, NASA Ames Research Center, April 2009.

[2]Rochelle, W. C., Battley, H. H., Grimaud, J. E., Tillian, D. J., Murray, L. P., Lueke, W. J., and Heaton, T. M., "Orbiter TPS Development and Certification Testing at the NASA/JSC 10 MW Atmospheric Reentry Materials and Structures Evaluation Facility," AIAA-83-0147, Jan. 1983.

[3]Balboni, J. A., Gökçen, T., Hui, F. C. L., Graube, P., Morrissey, P., Lewis, R. "Consolidating NASA's Arc-Jets," AIAA Paper 2015-2667, June 2015.

[4]Terrazas-Salinas, I., Carballo, J. E., Driver, D. M., and Balboni, J. A., "Comparison of Heat Transfer Measurement Devices in Arc Jet Flows with Shear," AIAA Paper 2010-5053, June 2010.

[5]ASTM E457-96, "Standard Test Method for Measuring Heat-Transfer Rate Using a Thermal Capacitance (Slug) Calorimeter," American Society for Testing and Materials, Ocober 1996 (Reapproved 2002, originally published in 1972).

[6]ASTM E511-07, "Standard Test Method For Measuring Heat Flux Using a Copper-Constantan Circular Foil Heat-Flux Gage," American Society for Testing and Materials, December 2007 (original standard published in 1973).

[7]ASTM E598-96, "Standard Test Method for Measuring Extreme Heat-Transfer Rates from High-Energy Environments Using a Transient, Null-Point Calorimeter," American Society for Testing and Materials, December 1996 (Reapproved 2002, originally published in 1977).

[8]Wright, M. J., Candler, G. V., and Bose, D., "Data-Parallel Line Relaxation Method for the Navier-Stokes Equations," *AIAA Journal*, Vol. 36, No. 9, 1998, pp. 1603-1609.

[9]Wright, M. J., "Data-Parallel Line Relaxation Code, DPLR Version 4.02," Private Communication, June 2010.

[10]Park, C., *Nonequilibrium Hypersonic Aerothermodynamics*, John Wiley & Sons, Inc., New York, 1990, Chap. 4.

[11]Gökçen, T., Chen, Y. K., Skokova, K. A., and Milos, F. S., "Computational Analysis of Arc-Jet Stagnation Tests Including Ablation and Shape Change," *Journal of Thermophysics and Heat Transfer*, Vol. 24, No. 4, 2010, pp. 694-707; also AIAA Paper 2009-3596, June 2009.

[12]Gökçen, T., Balboni, J. A., and Alunni, A. I. "Computational Simulations of the 10-MW TP3 Arc-Jet Facility," AIAA Paper 2015-3103, June 2015.

[13]ASTM E637-05, "Standard Test Method for Calculation of Stagnation Enthalpy from Heat Transfer Theory and Experimental Measurements of Stagnation-Point Heat Transfer and Pressure," American Society for Testing and Materials, November 2005 (originally published in 1978).

Appendix: Repeatability and probe dwell time sensitivity for Gardon gage surveys for 6 conditions (Figs. A1-A6)

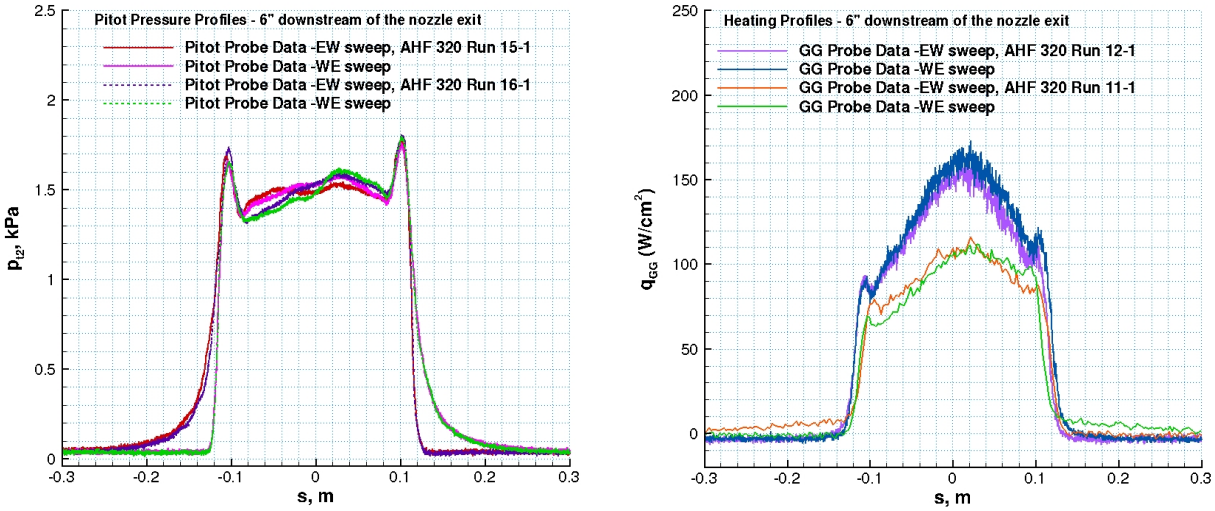

a) pitot pressure **b) heat flux**

Figure A1. Repeatability of the 15.9-mm probe measurements at different dwell times for condition 1. TP3 7.5-inch nozzle flow: $\dot{m}$ = 25 g/s, I = 279 A, p_{midc} = 27.5 kPa, p_{box} = 0.7-0.8 torr. The probe dwell times: 50 s for runs 15-1 aand 16-1, 1.2 s for run 11-1, 12 s for 12-1.

Note that the probe dwell time of 20 s for condition 1 in AHF 318 tests (not shown) was not sufficient to get reliable pitot pressure data.

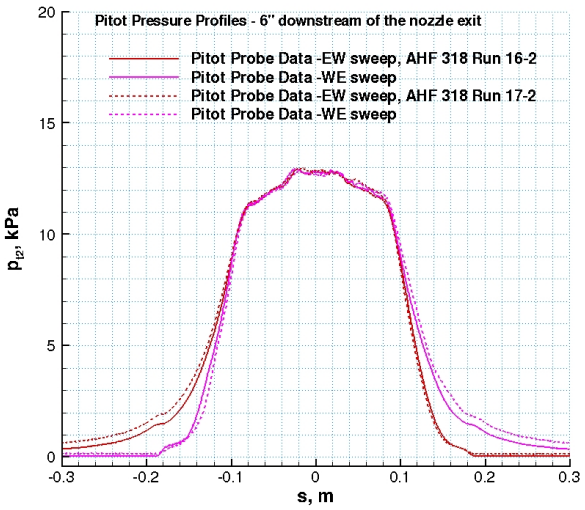

a) pitot pressure, AHF 318

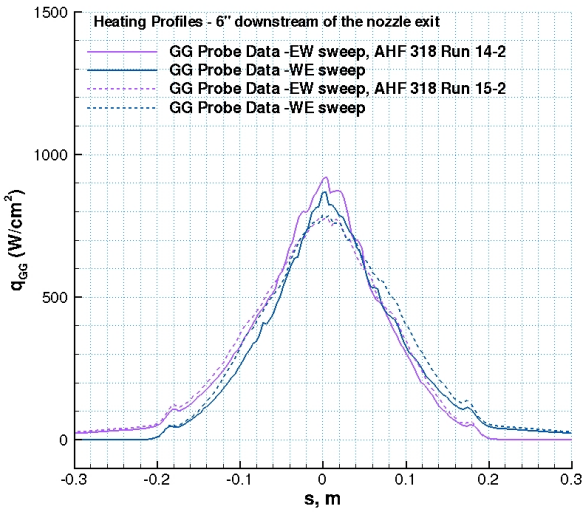

b) heat flux, AHF 318

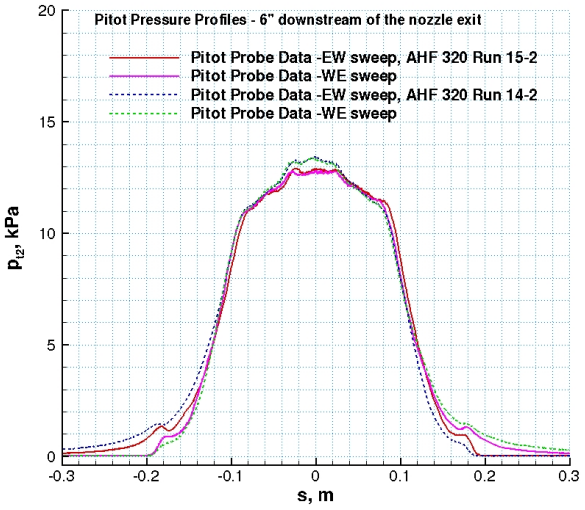

c) pitot pressure, AHF 320

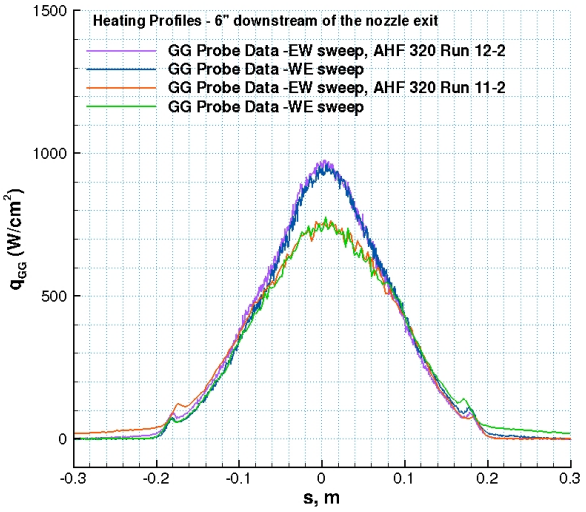

d) heat flux, AHF 320

Figure A2. Repeatability of the 15.9-mm probe survey measurements at different dwell times for condition 2. TP3 7.5-inch nozzle flow: $\dot{m}$ = 190 g/s, I = 1110 A, p_{midc} = 205 kPa, p_{box} = 0.4-1 torr. AHF 318 probe dwell times: 10 s for runs 16-2 and 17-2, 1.2 s for runs 14-2 and 15-2. AHF 320 probe dwell times: 15 s for run 14-2, 30 s for run 15-2, 1.6 s for run 11-2, and 7 s for 12-2.

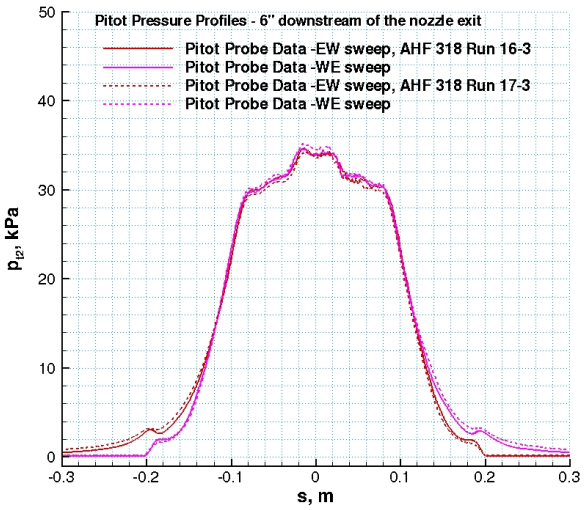

a) pitot pressure, AHF 318

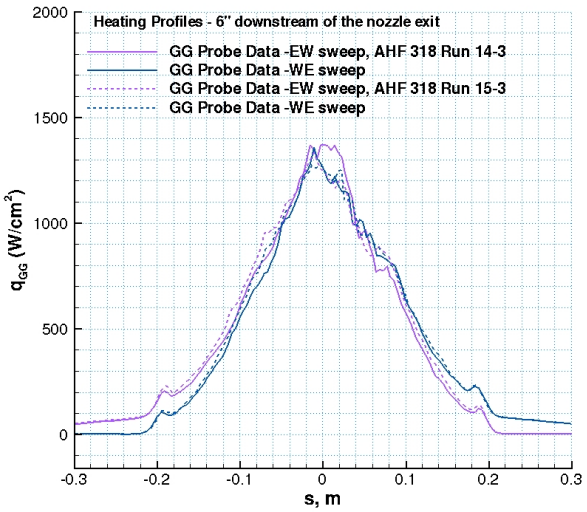

b) heat flux, AHF 318

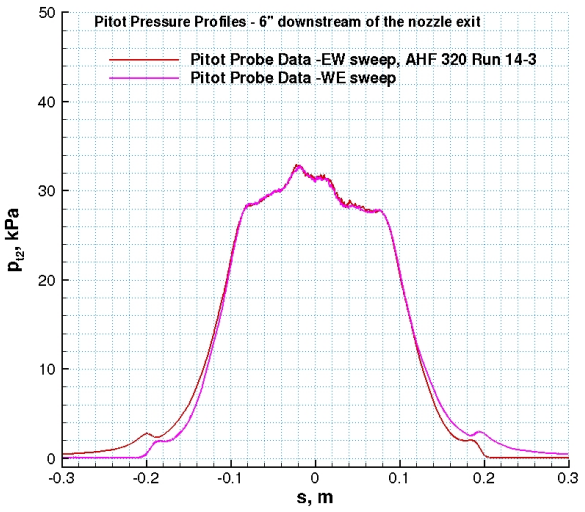

c) pitot pressure, AHF 320

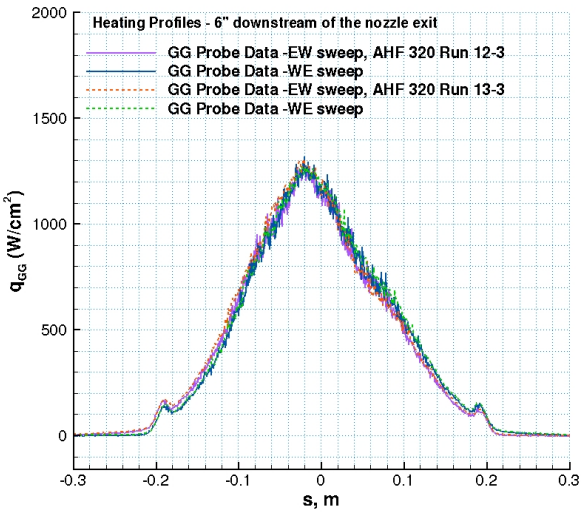

d) heat flux, AHF 320

Figure A3. Repeatability of the 15.9-mm probe survey measurements at different dwell times for condition 3. TP3 7.5-inch nozzle flow: $\dot{m}$ = 500 g/s, I = 1755 A, p_{midc} = 516-541 kPa, p_{box} = 0.4-1 torr. AHF 318 probe dwell times: 10 s for runs 16-3 and 17-3, 1.2 s for runs 14-3 and 15-3. AHF 320 probe dwell times: 15 s for run 14-3 (no repeat run), 7 s for runs 12-3 and 13-3.

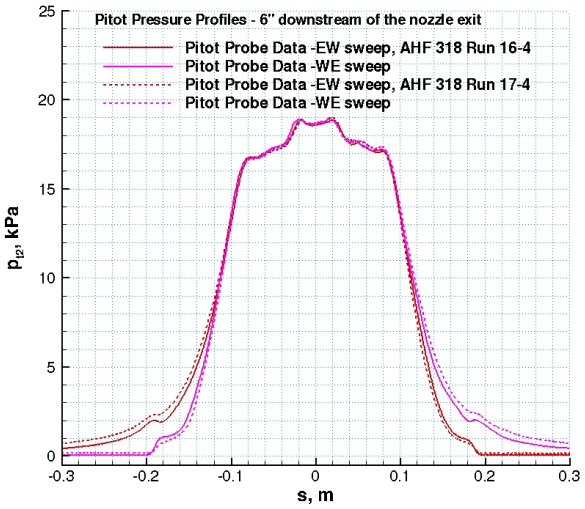

a) pitot pressure, AHF 318

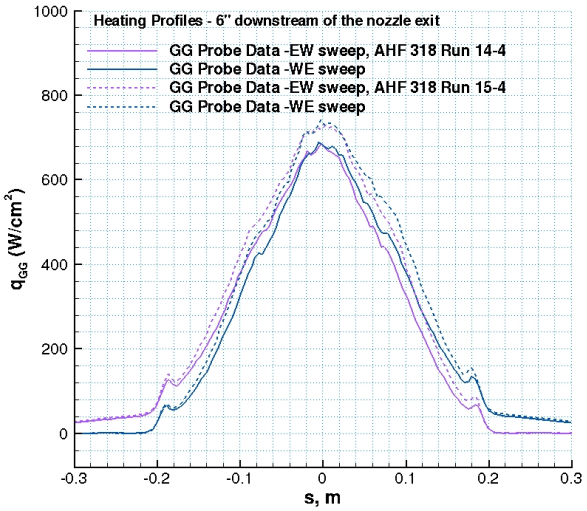

b) heat flux, AHF 318

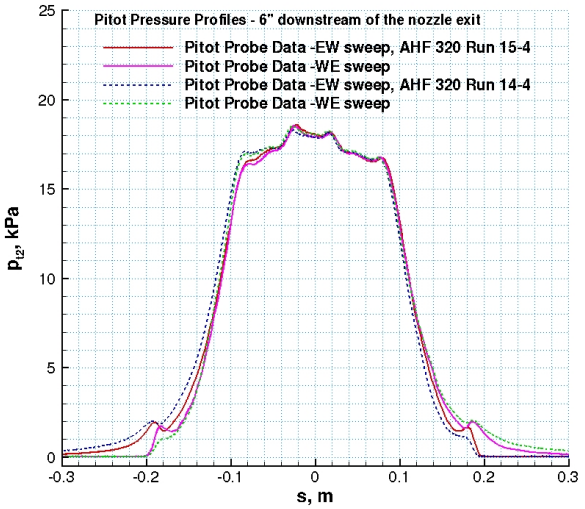

c) pitot pressure, AHF 320

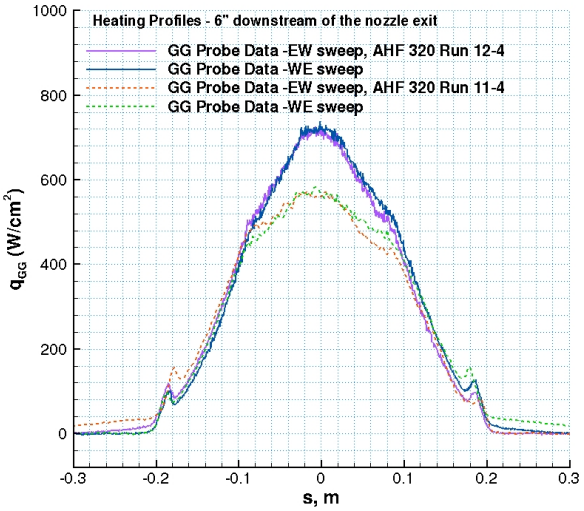

d) heat flux, AHF 320

Figure A4. Repeatability of the 15.9-mm probe survey measurements at different dwell times for condition 4. TP3 7.5-inch nozzle flow: $\dot{m}$ = 310 g/s, I = 1206 A, p_{midc} = 293-298 kPa, p_{box} = 0.4-1 torr. AHF 318 probe dwell times: 10 s for runs 16-4 and 17-4, 1.2 s for runs 14-4 and 15-4. AHF 320 probe dwell times: 15 s for run 14-4, 30 s for run 15-4 , 1.6 s for runs 11-4, and 7 s for run 12-4.

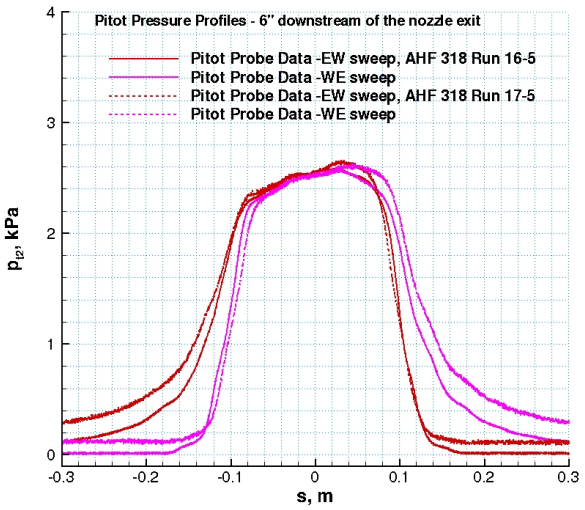

a) pitot pressure, AHF 318

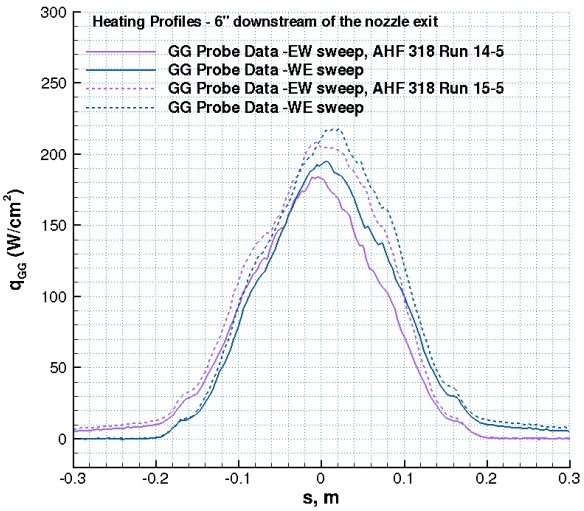

b) heat flux, AHF 318

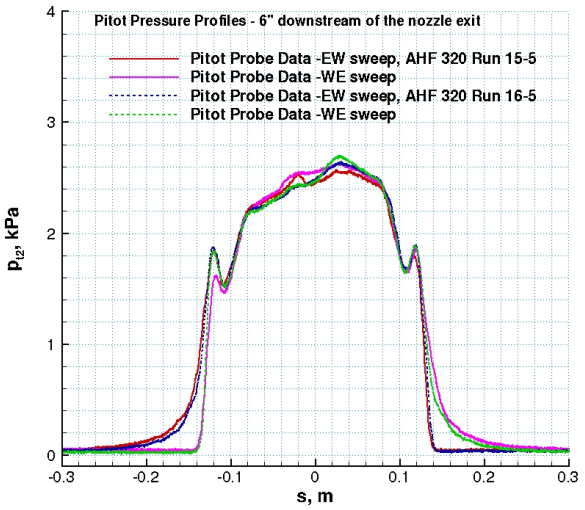

c) pitot pressure, AHF 320

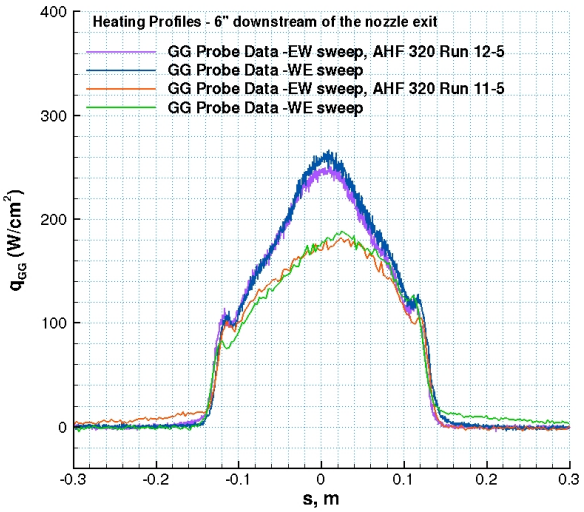

d) heat flux, AHF 320

Figure A5. Repeatability of the 15.9-mm probe survey measurements at different dwell times for condition 5. TP3 7.5-inch nozzle flow: $\dot{m}$ = 40 g/s, I = 415 A, p_{midc} = 40-43 kPa, p_{box} = 0.1-0.8 torr. AHF 318 probe dwell times: 20 s for runs 16-5 and 17-5, 1.2 s for runs 14-5 and 15-5. AHF 320 probe dwell times: 50 s for runs 15-5 and 16-5, 1.2 s for run 11-5 and 12 s for 12-5.

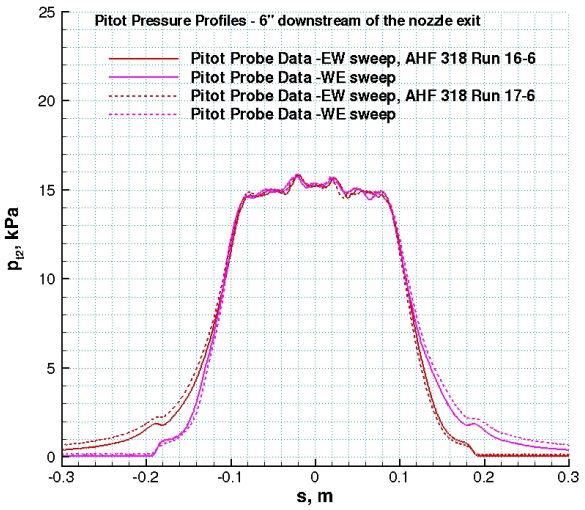

a) pitot pressure, AHF 318

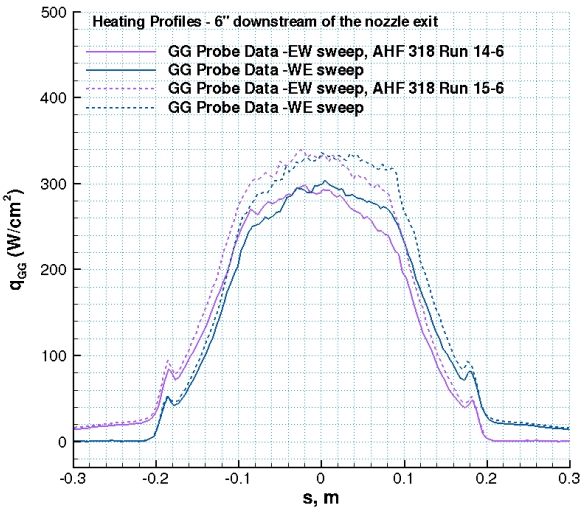

b) heat flux, AHF 318

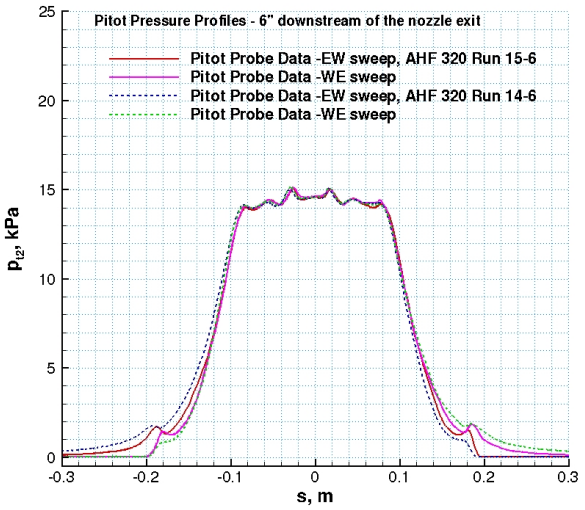

c) pitot pressure, AHF 320

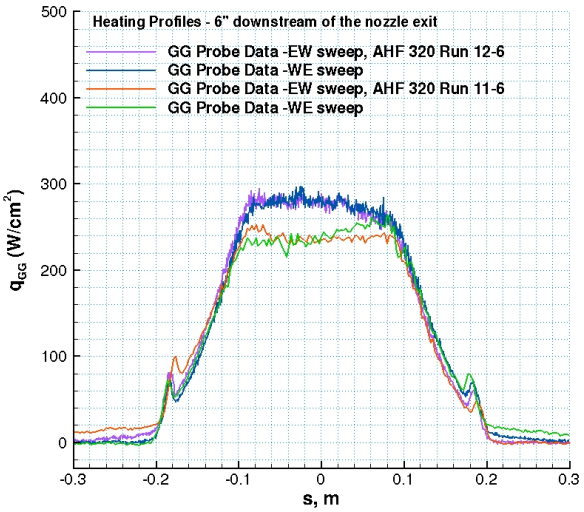

d) heat flux, AHF 320

Figure A6. Repeatability of the 15.9-mm probe survey measurements at different dwell times for condition 5. TP3 7.5-inch nozzle flow: $\dot{m}$ = 310 g/s, I = 710 A, p_{midc} = 240-248 kPa, p_{box} = 0.4-1 torr. AHF 318 probe dwell times: 10 s for runs 16-6 and 17-6, 1.2 s for runs 14-6 and 15-6. AHF 320 probe dwell times: 15 s for run 14-6, 30 s for 15-6, 1.6 s for run 11-6 and 7 s for 12-6.